Letters

Cost-Effective and Compact Multistring LED Driver Based on a Three-Coil Wireless Power Transfer System

Yong Li, Jiefeng Hu, *Senior Member, IEEE*, Xiaofei Li, Heshou Wang, and Ka Wai Eric Cheng

***Abstract*—In this letter, a multistring light-emitting diode (LED) driver based on a three-coil wireless power transfer system is proposed. The proposed system can solve the current imbalance problem among multiple LED strings because of its unique merit of multiple load-independent constant current (CC) outputs. Also, zero-phase-angle operation is achieved. Thus, not only the power rating of power switches can be reduced but also the efficiency is improved. For the sake of compactness, the source coil and the transmitter coil on the transmitting side are attached to the same plane. In addition, to further save the install space, magnetically integrated *LCL* resonators are utilized on the receiving side. The proposed system is cost-effective since only one receiver and passive components are needed to obtain the multiple CC outputs. Furthermore, by employing a master–slave control strategy, the output currents can be changed synchronously, which enables the "plug and play" capability and features a simple control structure. Finally, the feasibility of the proposed method is verified on a laboratory prototype.**

***Index Terms*—Constant current (CC), light-emitting diode (LED), three-coil, wireless power transfer (WPT).**

I. Introduction

OWING to the inherent advantages in lifespan, energy saving, and lighting efficiency, light-emitting diodes (LEDs) have been widely used in many applications, such as liquid crystal display back lighting, street lighting, general lighting, etc. [1]–[4]. Usually, due to the luminance limitation of a single LED, multiple LEDs connected in series are utilized for high-brightness applications. It is noted that, considering a safe accumulative forward voltage, the number of the series-connected LEDs is limited. Therefore, using multistring LEDs in parallel has become a common practice [5], [6]. Extensive research has shown that the luminosity of the LEDs relates to their forward currents. Thus, it has been widely recognized that LEDs should be

Manuscript received December 11, 2018; revised January 22, 2019; accepted February 8, 2019. Date of publication February 14, 2019; date of current version May 22, 2019. This work was supported in part by Hong Kong Polytechnic University under Grant 1-ZE7J, in part by Hong Kong Innovation and Technology Commission under Grant ITS/281/17, and in part by the Open Project of National Rail Transit Electrification and Automation Engineering Technique Research Center under Grant NEEC-2018-B05. *(Corresponding author: Xiaofei Li.)*

Y. Li is with the School of Electrical Engineering, Southwest Jiaotong University, Chengdu 610031, China, and also with the Department of Electrical Engineering, The Hong Kong Polytechnic University, Hong Kong (e-mail:

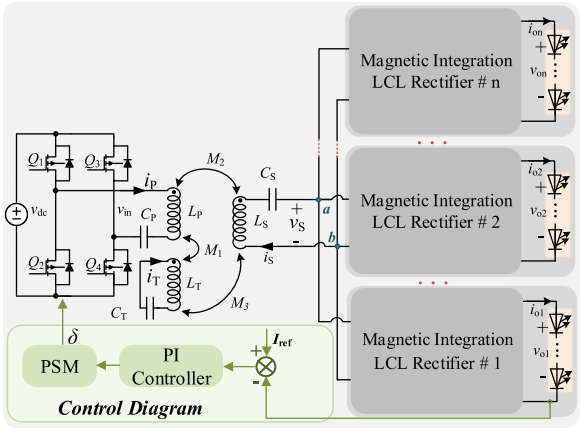

Fig. 1. Circuit diagram of the proposed WPT lighting system.

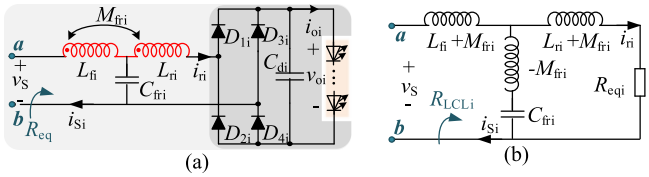

Fig. 2. Circuit diagram and coupled model of magnetic integration *LCL* rectifier #*i*. (a) Circuit diagram of *LCL* rectifier #*i*. (b) Decoupled model of *LCL* rectifier #*i*.

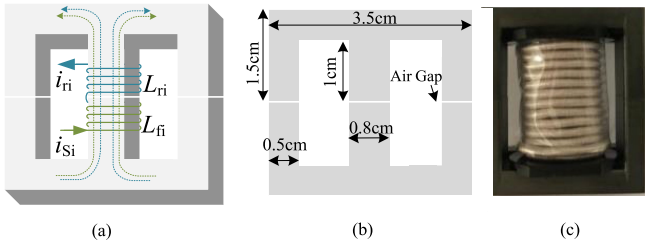

Fig. 3. (a) Schematic diagram of inductors. (b) Sizes of the inductor core from a front view. (c) Implementation of the coupled inductor.

configuration suffers from the following two major drawbacks: first, multiple receivers result in a large installation space; and second, all the receivers and their mutual inductances with the transmitter are expected to be identical. But the mutual inductance depends on the positions of the receivers, which, unfortunately, will vary when a misalignment occurs in practice.

Furthermore, to dramatically simplify the controller design, it is desirable that the output current of a WPT system is independent of the load. An analytical transformer modeling and compensation methods based on Boucherot bridge concept to design the WPT system are given in [13]. It is demonstrated that a WPT system with series–series (SS) or parallel–parallel compensation network presents current source behavior. A dc source output for driving LEDs by using SS compensation topology is given in [2]. The output current is load independent with the properly designed operating frequency. This proposed system is mainly for powering a single LED load. Nevertheless, the current imbalance between multistring LEDs is not mentioned.

To fill the aforementioned technical gap, a cost-effective and compact multistring LED driver based on a three-coil WPT system with only one receiver is proposed. The proposed system can obtain efficient multiple load-independent CC outputs without current imbalance by using the three-coil WPT structure with multiple *LCL* resonators. Zero-phase-angle (ZPA) operation of the whole system can be achieved. The proposed system also features a simple control strategy, since the output currents are load independent. A master–slave control method is utilized to conduct the closed-loop control, which makes the system features "plug and play" of the slave channels. The feasibility of the proposed method is finally verified by a laboratory prototype.

In contrast to traditional methods, this proposed approach is more superior. Compared with the method presented in [2], the proposed method is more applicable since the proposed method can obtain multiple load-independent CC outputs to supply multiple LED strings without current imbalance. Compared with the method presented in [11], the proposed approach is more efficient due to the fact that no dc/dc converts are needed to regulate the outputs. Compared with the method proposed in [8], the proposed approach is more compact and cost-effective since only one receiver is needed to obtain the multiple CC outputs.

II. Circuit Topology

Fig. 1 shows the proposed multistring LED driver based on a series–series–series compensated three-coil WPT system. L_P, L_T, and L_S are the self-inductances of the source coil, the transmitter coil, and the receiver coil, respectively. M_1, M_2, and M_3 are the mutual inductances among these three coils. Since L_P is smaller due to the less number of turns in the source coil compared to the other two coils, M_2 can be negligible, i.e., $M_2 = 0$ [10]. Moreover, the parasitic resistances of the coils can be neglected as well because they are relatively small by using high-quality Litz wire [14].

The inverter is controlled by using phase-shifted modulation (PSM) [15], and the fundamental output voltage in the phasor form can be given as

$$\dot{V}_{\rm in} = \frac{2\sqrt{2}V_{\rm dc}}{\pi}\sin\frac{\delta}{2}\angle 0^\circ \tag{1}$$

where δ is the conduction angle.

In order to drive multistring LEDs with CC outputs, modularized magnetic integration *LCL* rectifiers are utilized. As shown in Fig. 1, they are connected in parallel to a single receiver at ports *a* and *b*, i.e., fed by the common voltage $\dot{V}_{\rm S}$.

Taking the *i*th ($i = 1, 2, \ldots, n$) *LCL* rectifier for example, its circuit diagram is detailed in Fig. 2(a). The *LCL* rectifier consists of an *LCL* compensation network and a diode rectifier. For the *LCL* network, $L_{\rm fi}$ and $L_{\rm ri}$ are coupled with each other and the mutual inductance is $M_{\rm fri}$. It can be further equivalent to the decoupled model shown in Fig. 2(b). The equivalent impedance of *i*th LED string can be simplified as a load R_{oi} [5]. As a result, the input impedance of the *i*th rectifier including the *i*th LED string satisfies $R_{\rm eqi} = 8R_{oi}(\pi^2)^{-1}$ [15]. The construction of these modularized magnetic *LCL* structures is illustrated in Fig. 3(a). It shows that the two inductors are twined on the central limbs of EE cores, i.e., they are magnetically integrated [16]. The sizes of the inductor cores are shown in Fig. 3(b), and the implementation is shown in Fig. 3(c). This integration structure is favorable for the compact modular design as additional install space is not needed [17].

C_P, C_T, and C_S shown in Fig. 1 and $C_{\rm fri}$ ($i = 1, 2, \ldots, n$) shown in Fig. 2 are the resonant capacitors, which satisfy the following equation:

$$\begin{cases} C_{\rm P} = (\omega^2 L_{\rm P})^{-1} C_{\rm S} = (\omega^2 L_{\rm S})^{-1} C_{\rm T} = (\omega^2 L_{\rm T})^{-1} \\ C_{\rm fri} = (\omega^2 L_{\rm fi})^{-1} C_{\rm fri} = (\omega^2 L_{\rm ri})^{-1} \end{cases} \tag{2}$$

where ω is the operating frequency of the proposed WPT system.

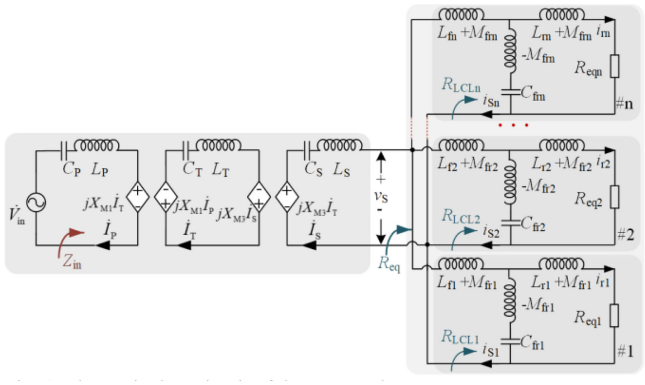

Fig. 4. Equivalent circuit of the proposed system.

Then, by using Kirchhoff voltage law (KVL) in Fig. 2(b), the following equations can be derived:

$$\begin{cases} \dot{V}_S = (jX_{\mathrm{Lfi}} + jX_{\mathrm{Mfri}})\,\dot{I}_{\mathrm{Si}} + \left(\dot{I}_{\mathrm{Si}} - \dot{I}_{\mathrm{ri}}\right)(jX_{\mathrm{Cfri}} - jX_{\mathrm{Mfri}}) \\ 0 = \left(\dot{I}_{\mathrm{ri}} - \dot{I}_{\mathrm{Si}}\right)(jX_{\mathrm{Cfri}} - jX_{\mathrm{Mfri}}) + (jX_{\mathrm{Lri}} + jX_{\mathrm{Mfri}} + R_{\mathrm{eq1}})\,\dot{I}_{\mathrm{ri}} \end{cases} \tag{3}$$

where

$$\begin{cases} X_{\mathrm{Lfi}} = \omega L_{\mathrm{fi}} & X_{\mathrm{Lri}} = \omega L_{\mathrm{ri}} \\ X_{\mathrm{Mfri}} = \omega M_{\mathrm{fri}} & X_{\mathrm{Cfri}} = 1/\omega C_{\mathrm{fri}}. \end{cases} \tag{4}$$

Substituting (2) and (4) into (3), the output current $\dot{I}_{\mathrm{ri}}$ and the input resistance R_{LCLi} can be calculated as

$$\dot{I}_{\mathrm{ri}} = \dot{V}_S / j\omega\,(L_{\mathrm{fi}} + M_{\mathrm{fri}}) \tag{5}$$

$$R_{LCLi} = \dot{V}_S / \dot{I}_{\mathrm{Si}} = (\omega L_{\mathrm{fi}} + \omega M_{\mathrm{fri}})^2 / R_{\mathrm{eqi}}. \tag{6}$$

From (5), it can be seen that $\dot{I}_{\mathrm{ri}}$ is independent of the load. It can be kept constant as long as $\dot{V}_S$ is a constant voltage since L_{fi} and M_{fri} are usually fixed. Equation (5) also reveals another advantage of the integrated structure. That is, for achieving the same output current, the inductance of the coupled inductor will be smaller, compared with that without coupling.

Now, the complete equivalent circuit of the proposed WPT system is shown in Fig. 4, where Z_{in} is the equivalent input resistance. R_{eq} is the equivalent impedance of the paralleled *LCL* rectifiers, which can be expressed as

$$R_{\mathrm{eq}} = R_{LCL1} \,\|R_{LCL2}\| \ldots \| R_{LCLn}. \tag{7}$$

Since R_{LCLi} is purely resistive, it is easy to derive that R_{eq} is purely resistive as well.

Then, according to KVL, the following equations can be derived:

$$\begin{cases} \dot{V}_{\mathrm{in}} = (jX_{\mathrm{LP}} + jX_{\mathrm{CP}})\,\dot{I}_P + jX_{M1}\dot{I}_T \\ 0 = jX_{M1}\dot{I}_P + (jX_{\mathrm{LT}} + jX_{\mathrm{CT}})\,\dot{I}_T - jX_{M3}\dot{I}_S \\ 0 = -jX_{M3}\dot{I}_T + (jX_{\mathrm{LS}} + jX_{\mathrm{CS}} + R_{\mathrm{eq}})\,\dot{I}_S \\ \dot{V}_S = R_{\mathrm{eq}}\dot{I}_S \end{cases} \tag{8}$$

where

$$\begin{cases} X_{\mathrm{LP}} = \omega L_P \;\; X_{\mathrm{LT}} = \omega L_T \;\; X_{\mathrm{LS}} = \omega L_S \;\; X_{M1} = \omega M_1 \\ X_{\mathrm{CP}} = 1/\omega C_P \;\; X_{\mathrm{CT}} = 1/\omega C_T \;\; X_{\mathrm{CS}} = 1/\omega C_S \;\; X_{M2} = \omega M_2. \end{cases} \tag{9}$$

Substituting (2) and (9) into (8), one can obtain

$$\dot{I}_T = \dot{V}_{\mathrm{in}}/j\omega M_1 \;\; \dot{V}_S = \dot{V}_{\mathrm{in}} M_3/M_1 \;\; Z_{\mathrm{in}} = {M_1}^2 R_{\mathrm{eq}}/{M_3}^2. \tag{10}$$

From (10), it is clear that both the output current $\dot{I}_T$ of the transmitter coil and the output voltage $\dot{V}_S$ of the receiver are load independent. Moreover, according to (7), it can be seen that Z_{in} is purely resistive. Therefore, the ZPA of the whole system can be achieved.

According to [14], the relationship between the input and output currents of the *i*th rectifier can be expressed as

$$I_{\mathrm{ri}} = \frac{\pi\sqrt{2}}{4} I_{oi}. \tag{11}$$

Then, by substituting (1), (5), and (10) into (11), the dc of the *i*th LED string can be derived as

$$I_{oi} = \frac{8M_3 V_{\mathrm{dc}} \sin\frac{\delta}{2}}{\pi^2 \omega M_1\,(L_{\mathrm{fi}} + M_{\mathrm{fri}})} \quad i = 1, 2, \ldots, n. \tag{12}$$

It is obvious from (12) that the currents of respective LED strings are irrelevant to the LED loads. Instead, they are determined by ω, V_{dc}, δ, M_1, M_3, and the corresponding L_{fi}, M_{fri} $(i = 1, 2, \ldots, n)$ of the *LCL* resonators. Furthermore, (12) shows that the output current of each channel is independent of each other, which means the cross-talk effect can be negligible. Besides, by individually adjusting L_{fi}, M_{fri} of the *i*th *LCL* resonator, different current levels can be generated. This feature is suitable for powering multistring LEDs with different current ratings. For simplicity, the specifications of multistring LEDs are considered to be the same, i.e., the required multiple currents are identical; thus, L_{fi} and M_{fri} $(i = 1, 2, \ldots, n)$ of the *LCL* resonators are selected to be the same, respectively.

III. System Control and Discussion

In some situations, it is necessary to change the luminance of the LED lighting system. Therefore, the output currents should be regulated synchronously to that in [18] and [19]. The proposed closed-loop control diagram is illustrated in Fig. 1, where δ is the control variable. Since output currents change synchronously with the control variable δ according to (12), only one feedback control loop is needed. The controlled channel (#1) can be assigned as master channel while others serve as slave channels. The error between the sensed current I_{o1} and the reference I_{ref} is sent to the proportion-integral controller. Then, the processed result is delivered to the PSM controller for the calculation of conduction angle δ. Since the output currents of the slave channels change synchronously with those of the master channel, the current balancing of the proposed system can thus be easily achieved.

It should be noted that the slave channels cannot be controlled if the master channel fails. This is the inherent characteristic of the master–slave control strategies. However, the proposed system features the "plug and play" capability, which facilitates flexible expansion or reduction of LED strings in practice.

IV. Experimental Verifications

A laboratory prototype with one master channel and one slave channel is built, as shown in Fig. 5. The source coil and the transmitter coil are attached to the top and the bottom of the same plane. Two LED strings with 12 CA-F133 series LEDs are used for evaluations. The rated current of each LED is 1 A with voltage fall of 3.6 V at 25 °C. The parameters of the system are listed in Table I.

Fig. 6 shows the key waveforms of the inverter at the primary side and the output currents at the receiver side. It can be seen that v_{in} and i_P are almost in phase, indicating ZPA operation and hence reduced

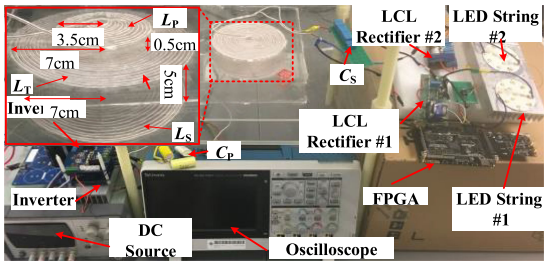

Fig. 5. Experimental setup.

TABLE I
SYSTEM PARAMETERS

V_{dc}	L_P	L_T	L_S	M_1	M_3
60 V	4.59 μH	32.77 μH	29.86 μH	4.25 μH	6.74 μH
C_P	C_T	C_S	L_{f1}	L_{r1}	C_{fr1}
137.05 nF	19.32 nF	21.10 nF	45.02 μH	45.10 μH	13.98 nF
L_{f2}	L_{r2}	C_{fr1}	M_{fr1}	M_{fr2}	f
45.05 μH	45.07 μH	13.97 nF	42.69 μH	42.67 μH	200 kHz

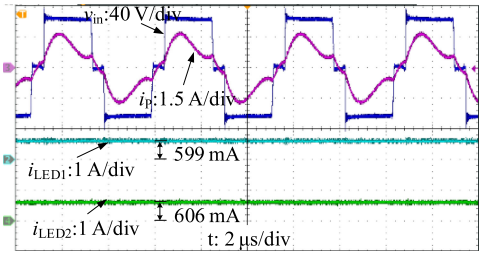

Fig. 6. Key waveforms of the inverter and the waveforms of the output currents.

conduction loss. The output currents of the master channel (i_{LED1}) and the slave channel (i_{LED2}) are controlled closely to the reference 600 mA, showing good current balancing capability. The measured overall efficiency (dc–dc efficiency) is about 88% in this case.

Fig. 7 depicts the output voltage and current waveforms of the master channel and the slave channel when the loaded number of LEDs varies by short-connecting the specified number of LEDs. Specifically, Fig. 7(a) indicates that the number of series-connected LEDs at the master channel (n_m) changes from 12 to 10 and back to 12, whereas Fig. 7(b) indicates that the number of series-connected LEDs at the slave channel (n_s) changes from 12 to 10 and back to 12. From Fig. 7(a), it can be seen that i_{LED1} can be maintained at a steady state of 600 mA with a slight overshoot when n_m changes from 12 to 10 and back to 12. i_{LED2} is kept at 600 mA regardless of the variations of n_m. Similar results can be observed in Fig. 7(b). When n_s changes from 12 to 10 and back to 12, i_{LED2} can be maintained at a steady state of 600 mA with a slight overshoot, while i_{LED1} is stable at 600 mA regardless of the variations of n_s. The results demonstrate that the variation in loaded LEDs of the slave channel would not affect the master channel, which is consistent with the theoretical analysis.

Fig. 8 shows the dynamic tracking process when the reference current I_{ref} changes from 600 to 400 mA and back to 600 mA. It can be observed that the output currents i_{LED1} and i_{LED2} decrease from 600 to 400 mA, with a fast transient of 80 ms, and rise from 400 to 600 mA with a response time of 120 ms. This change synchronism agrees well with the theoretical analysis, and the fast transient response shows the good controllability of the closed-loop control method.

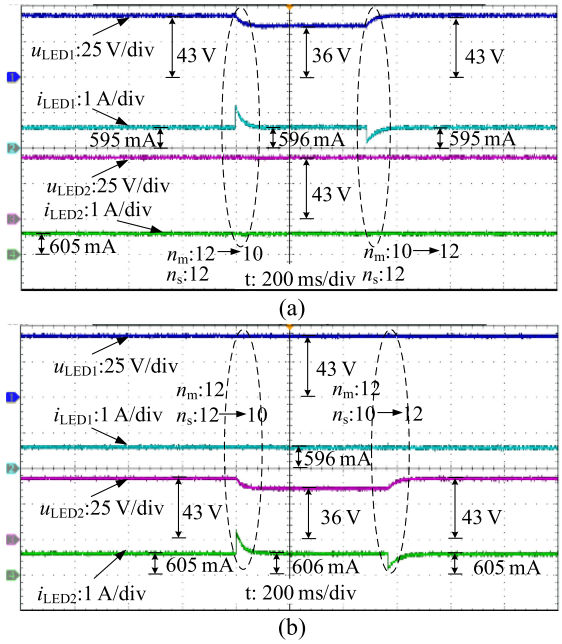

Fig. 7. Dynamic performance of the proposed WPT system. (a) When n_m changes from 12 to 10 and back to 12. (b) When n_s changes from 12 to 10 and back to 12.

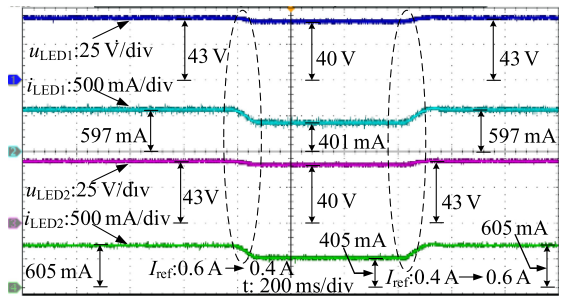

Fig. 8. Dynamic tracking process when I_{ref} changes.

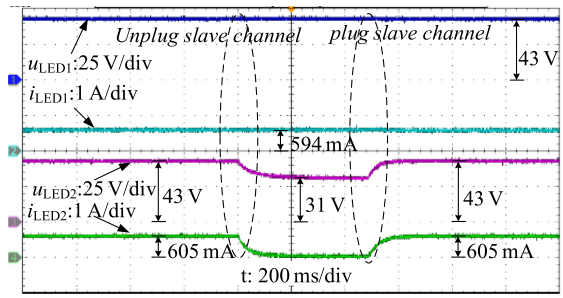

Fig. 9. Experimental results of "plug and play" of the slave channel.

The experimental results in terms of "plug and play" of the slave channel are shown in Fig. 9. It is seen that the plugging or unplugging of the slave channel does not affect the master channel. This advantage facilitates flexible expansion or reduction of LED strings in practice. As expected, the output current i_{LED2} of the slave channel becomes zero when the slave channel is unplugged. But the output voltage u_{LED2} decreases to 31 V rather than dropping down to zero due to the stored energy of the dc capacitor. This is also attributed to

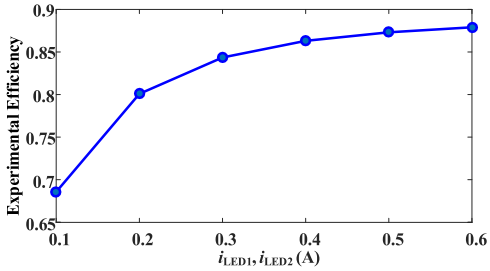

Fig. 10. Experimental efficiencies with different output currents.

a large equivalent resistor of the LEDs when the forward current is zero.

The experimental efficiencies with different output currents i_{LED1}, i_{LED2} are shown in Fig. 10. The efficiency increases with the increase in output current i_{LED1}, i_{LED2}, and it reaches 88% when $i_{\mathrm{LED1}} = i_{\mathrm{LED2}} = 600$ mA.

V. Conclusion

A multistring LED driver based on a three-coil WPT system is proposed. Multiple load-independent CC outputs are obtained by using multiple *LCL* resonators to avoid current imbalance. The system is compact since that the source coil and the transmitter coil are attached in the same plane at the primary side and the magnetically integrated *LCL* resonators are utilized at the receiving side with only one receiving coil. A master–slave control method is developed to conduct the closed-loop control, which endows the system with "plug and play" capability. An experimental prototype is built to verify the feasibility of the proposed approach, and the experimental results show good consistency with the theoretical analysis.

References

[1] S. Li, S. C. Tan, C. K. Lee, E. Waffenschmidt, S. Y. R. Hui, and C. K. Tse, "A survey, classification, and critical review of light-emitting diode drivers," *IEEE Trans. Power Electron.*, vol. 31, no. 2, pp. 1503–1516, Feb. 2016.

[2] X. Qu, W. Zhang, S. C. Wong, and C. K. Tse, "Design of a current-source-output inductive power transfer LED lighting system," *IEEE J. Emerg. Sel. Topics Power Electron.*, vol. 3, no. 1, pp. 306–314, Mar. 2015.

[3] Y. Zhou, S. Qian, Z. Qi, L. Huang, and A. P. Hu, "A simple brightness and color control method for LED lighting based on wireless power transfer," *IEEE Access*., vol. 6, pp. 51477–51483, 2018.

[4] J. Kuipers, H. Bruning, S. Bakker, and H. Rijnaarts, "Transformer-isolated resonant driver for parallel strings with robust balancing and stabilization of individual led current," *IEEE Trans. Power Electron.*, vol. 29, no. 7, pp. 3694–3708, Jul. 2014.

[5] X. Qu, S. C. Wong, and C. K. Tse, "An improved LCLC current-source-output multistring LED driver with capacitive current balancing," *IEEE Trans. Power Electron.*, vol. 30, no. 10, pp. 5783–5791, Oct. 2015.

[6] X. Qu, S. C. Wong, and C. K. Tse, "A current balancing scheme with high luminous efficacy for high-power LED lighting," *IEEE Trans. Power Electron.*, vol. 29, no. 6, pp. 2649–2654, Jun. 2014.

[7] K. H. Loo, Y. M. Lai, and C. K. Tse, "Design and analysis of LCC resonant network for quasi-lossless current balancing in multistring AC-LED array," *IEEE Trans. Power Electron.*, vol. 28, no. 2, pp. 1047–1059, Feb. 2013.

[8] R. Zhou, H. Chung, and R. Zhang, "An inductive power transfer system for driving multiple OLED light panels," *IEEE Trans. Power Electron.*, vol. 31, no. 10, pp. 7131–7147, Oct. 2016.

[9] W. X. Zhong, C. Zhang, X. Liu, and S. Y. R. Hui, "A methodology for making a three-coil wireless power transfer system more energy efficient than a two-coil counterpart for extended transfer distance," *IEEE Trans. Power Electron.*, vol. 30, no. 2, pp. 933–942, Feb. 2015.

[10] J. Zhang, X. Yuan, C. Wang, and Y. He, "Comparative analysis of two-coil and three-coil structures for wireless power transfer," *IEEE Trans. Power Electron.*, vol. 32, no. 1, pp. 341–352, Jan. 2017.

[11] V. B. Vu, V. T. Phan, D. T. Nguyen, T. Logenthiran, and R. T. Naayagi, "Design and implementation of a multi-output inductive charger for electric vehicles," in *Proc. Int. Conf. Sustain. Energy Technol.*, 2016, pp. 414–419.

[12] M. Liu, M. Fu, Y. Wang, and C. Ma, "Battery cell equalization via megahertz multiple-receiver wireless power transfer," *IEEE Trans. Power Electron.*, vol. 33, no. 5, pp. 4135–4144, May 2018.

[13] K. Woronowicz, A. Safaee, and T. R. Dickson, "Single-phase zero reactive power wireless power transfer topologies based on Boucherot bridge circuit concept," *Can. J. Elect. Comput. Eng.*, vol. 38, no. 4, pp. 323–337, Fall 2015.

[14] Y. Li, Q. Xu, T. Lin, J. Hu, Z. He, and R. Mai, "Analysis and design of load-independent output current or output voltage of a three-coil wireless power transfer system," *IEEE Trans. Transp. Electrific.*, vol. 4, no. 2, pp. 364–375, Jun. 2018.

[15] Y. Li, J. Hu, F. Chen, Z. Li, Z. He, and R. Mai, "Dual-phase-shift control scheme with current-stress and efficiency optimization for wireless power transfer systems," *IEEE Trans. Circuits Syst. I, Reg. Papers*, vol. 65, no. 9, pp. 3110–3121, Sep. 2018.

[16] J. Fang, H. Li, and Y. Tang, "A magnetic integrated LLCL filter for grid-connected voltage-source converters," *IEEE Trans. Power Electron.*, vol. 32, no. 3, pp. 1725–1730, Mar. 2017.

[17] W. Li., H. Zhao, S. Li, J. Deng, T. Kan, and C. C. Mi, "Integrated LCC compensation topology for wireless charger in electric and plug-in electric vehicles," *IEEE Trans. Ind. Electron.*, vol. 62, no. 7, pp. 4215–4225, Jul. 2015.

[18] J. Zhang, L. Xu, X. Wu, and Z. Qian, "A precise passive current balancing method for multioutput LED drivers," *IEEE Trans. Power Electron.*, vol. 26, no. 8, pp. 2149–2159, Aug. 2011.

[19] X. Chen, D. Huang, Q. Li, and F. C. Lee, "Multichannel LED driver with CLL resonant converter," *IEEE J. Emerg. Sel. Topics Power Electron.*, vol. 3, no. 3, pp. 589–598, Sep. 2015.